Magnetic coupling at interface of ultrathin Co film and antiferromagnetic $Cr_2O_3(0001)$ film

Cite as: J. Appl. Phys. **106**, 033903 (2009); https://doi.org/10.1063/1.3182802
Submitted: 13 April 2009 • Accepted: 22 June 2009 • Published Online: 04 August 2009

Yu Shiratsuchi, Toshihiro Nakatani, Shin-ichi Kawahara, et al.

Magnetic coupling at interface of ultrathin Co film and antiferromagnetic $Cr_2O_3(0001)$ film

Yu Shiratsuchi,[a] Toshihiro Nakatani, Shin-ichi Kawahara, and Ryoichi Nakatani
Department of Materials Science and Engineering, Graduate School of Engineering, Osaka University, 2-1 Yamadaoka, Suita, Osaka 565-0871, Japan

(Received 13 April 2009; accepted 22 June 2009; published online 4 August 2009)

The magnetic coupling at the interface of Co and Cr has been investigated using ultrathin Co film on $Cr_2O_3(0001)$ film, which is expected to be a promising system to show the magnetoelectronic effect. We mainly examined the temperature dependence of magnetization, the exchange bias at different field directions relative to the Cr spin direction, and the temperature dependence of exchange bias. The temperature dependence of magnetization under 50 Oe indicates the collinear coupling of Co spin and Cr spin at the interface. Furthermore, the exchange bias effect is observed in the coupled direction of Co and Cr, namely, parallel to the Cr spin direction. However, the changes in the magnetic behavior with changing field directions and Co thicknesses imply the existence of biquadratic coupling of Co spin and Cr spin, as well. In agreement with the numerical calculation under the coexistence of collinear and biquadratic couplings, the exchange bias field decreases nonmonotonically with increasing temperature. © *2009 American Institute of Physics*. [DOI: 10.1063/1.3182802]

I. INTRODUCTION

Controlling the magnetization direction of nanosized magnets is an attractive issue from an engineering viewpoint partly because the magnetization direction governs the performance of some types of magnetic devices. The magnetization direction is determined by magnetic anisotropy at low or zero magnetic fields, thus control of the magnetization direction is achieved by controlling the magnetic anisotropy. Particularly for the nanosized magnet, the surface/interface contribution to effective magnetic anisotropy becomes significant because of the large surface-to-volume ratio. From this viewpoint, we have been investigating the control of the magnetic anisotropy of a nanosized magnet using the surface/interface effect.[1,2] Among the various types of surface/interface effects, we focus on the interface anisotropy between a ferromagnet and the antiferromagnet, known as exchange anisotropy.

In order to control the magnetization direction, the magnetization must be fixed to a certain direction. However, the magnetization of a nanosized magnet fluctuates as a result of the thermal agitation owing to its tiny volume.[1] As is well known, to fix the magnetization direction against thermal agitation, it is necessary to increase the magnetic anisotropy energy. Since the exchange anisotropy acts as an additional source of magnetic anisotropy, it contributes to the improvement of the thermal stability of the magnetization of nanosized magnets as well. In fact, it is reported that the thermal stability of magnetic nanoparticles in a granular film is drastically improved by using exchange anisotropy at the Co/CoO interface.[3]

It is known that the direction of exchange anisotropy depends on the spin direction of the antiferromagnet at the interface.[4] Thus, for the above purpose, an antiferromagnet possessing uniaxial anisotropy is suitable for controlling the spin direction at the interface. α-Cr_2O_3 has the corundum structure and possesses uniaxial anisotropy parallel to the c-axis.[5] This feature enables us to control the spin direction by altering the crystallographic orientation of α-Cr_2O_3. Additionally, the exchange anisotropy using α-Cr_2O_3 attracted much attention from the viewpoint that it is electrically controllable through the magnetoelectronic effect.[6]

It is also known that the exchange anisotropy is affected by some types of magnetic coupling of a ferromagnet to an antiferromagnet at the interface.[7,8] Particularly for an oxide antiferromagnet such as α-Cr_2O_3, two types of ferromagnet to antiferromagnet coupling are expected, namely, direct exchange coupling and superexchange coupling through an oxygen ion. In fact, there is a report indicating that the exchange bias and coercivity enhancement are dominated by different mechanisms[4] and the above two types of coupling mechanisms can act as the different origins. In this study, we address the magnetic coupling of ultrathin magnetic film and α-Cr_2O_3 at the interface using Co as a ferromagnet. Note that Co can possess the fcc or hcp structure, both of which can be epitaxially grown on α-Cr_2O_3. In this study, we mainly examine the temperature dependence of magnetization and the exchange bias effect of ultrathin Co film on α-Cr_2O_3, including the dependences of field direction and temperature. We will discuss the magnetic coupling of Co to Cr spin at the interface on the basis of the obtained results.

II. EXPERIMENTAL PROCEDURES

The samples were fabricated by molecular beam epitaxy (MBE) using a VG Semicon V80M multichamber MBE system under a base pressure below 5×10^{-9} Pa. Prior to the thin film growth, the substrate of mirror-polished Si(111) wafer was annealed at 1173 K for 120 s twice to obtain a clean

[a]Author to whom correspondence should be addressed. Tel./FAX: +81-6-6879-7489. Electronic mail: shiratsuchi@mat.eng.osaka-u.ac.jp.

and smooth surface. The surface structures and smoothness were confirmed by reflection high-energy electron diffraction (RHEED). Then, a 100-nm-thick Ag(111) buffer layer was grown on the Si(111) substrate at 273 K. The Ag buffer layer was subsequently annealed for 3.6 ks at 673 K to smooth the surface. Furthermore, a 20-nm-thick Au(111) base layer was epitaxially grown on the Ag(111) buffer layer at 373 K as an underlayer of α-Cr_2O_3 film. α-Cr_2O_3 film was fabricated by oxidizing Cr(110) film in a high-purity O_2 atmosphere. 20-nm-thick Cr(110) films were grown on the Au(111) base layer at 373 K. Then, the sample was transferred to the oxidization chamber in the MBE multichamber system and was annealed for 1.8 ks at 1073 K in high-purity O_2 gas flow. The O_2 gas pressure during annealing was controlled at 3×10^{-3} Pa. The oxygen concentration of the oxidized Cr film was confirmed using an energy dispersion x-ray (EDX) microanalyzer. The concentration ratio of Cr/O was determined to be $37.6/62.4 \approx 0.60$. Hence, it is roughly identical to stoichiometric α-Cr_2O_3, although the oxygen concentration is slightly low.

After transferring the sample back to the growth chamber, 2.3-nm-thick or 1.0-nm-thick Co was grown on the α-Cr_2O_3 film at 473 K. Since some structural and magnetic characterizations were performed *ex situ*, namely, after taking the sample from the UHV chamber, the samples are unavoidably exposed to air. To prevent the surface oxidization of Co, 4.0-nm-thick Cr and 6.0-nm-thick Au films were deposited on Co film at 293 K as the capping layer.

RHEED observations were conducted to characterize the surface structure of each layer and substrate. RHEED observations were carried out *in situ* at 30 kV with an incident angle of about 1°. The crystal orientations perpendicular to the film surface were determined from the RHEED observations. The crystal orientation relationship among the Si substrate, Au base layer, and α-Cr_2O_3 film were determined by the x-ray diffraction (XRD) method. The surface roughness of the α-Cr_2O_3 film was measured by means of atomic force microscopy (AFM). Magnetization measurements were performed by superconducting quantum interference device magnetometry. Our investigation encompassed the magnetization curve and the temperature dependence of magnetization in the temperature range of 5–340 K. Both types of measurements were carried out after both field cooling (FC) and zero-field cooling (ZFC). The remanent magnetization after FC, called thermoremanent magnetization (TRM), was also measured as a function of temperature. TRM was measured at zero magnetic field after cooling the sample in a field of 50 Oe.[9] These measurements were performed during the heating process after the samples were cooled from 340 to 5 K. Note that the Néel temperature, T_N, of bulk α-Cr_2O_3 is reported to be about 307 K,[10] and thus the samples were cooled through T_N. The magnetization was measured with the applied field direction both parallel and perpendicular to the film surface.

III. STRUCTURAL CHARACTERIZATION

As described in the last section, our Cr_2O_3 thin films were fabricated by oxidizing the metallic Cr film. In this process, the resultant structure of oxide film is not always a single-crystalline or oriented film, but often becomes polycrystalline or amorphous. In fact, we previously reported that the crystalline quality of the oxidized Cr film is affected by the in-plane epitaxial variants of Cr(110) film before oxidization.[11] As a main result of our previous report, it was found that the α-$Cr_2O_3(0001)$ film is successfully fabricated by oxidizing the threefold symmetric Cr(110) film. On the basis of these findings, Cr(110) film was prepared on Au(111) surface in this study. The threefold symmetry of Cr(110) owing to the Nishiyama–Wasserman relationship on the Au(111) base layer is confirmed from the RHEED patterns shown in Fig. 1(a) although the involvement of Kurdjumov–Sachs relationship is not completely ruled out. Note that Nishiyama–Wasserman relationship of Cr(110) and Au(111) is reported in the previous paper.[12] Upon oxidizing these films, RHEED patterns show a clear change. Figures 1(b) and 1(c) show the RHEED patterns after oxidization for different azimuths. Well-defined diffraction spots are observed and thus our Cr oxide films possess a highly oriented crystalline structure, which are neither polycrystalline nor amorphous. As shown in the corresponding key diagram, the observed diffraction patterns are indexed by the corundum structure having the (0001) orientation, indicating the formation of α-$Cr_2O_3(0001)$. While the $[1\bar{1}00]$ azimuth RHEED pattern is indexed by the single set of diffraction spots of α-$Cr_2O_3(0001)$ [Fig. 1(b)], the $[11\bar{2}0]$ azimuth RHEED pattern needs two sets of diffraction spots having mirror symmetry to each other, which are represented by the black circles, respectively, in the key diagram [Fig. 1(c)]. This means that our α-$Cr_2O_3(0001)$ has a twin boundary parallel to the $[11\bar{2}0]$ direction.

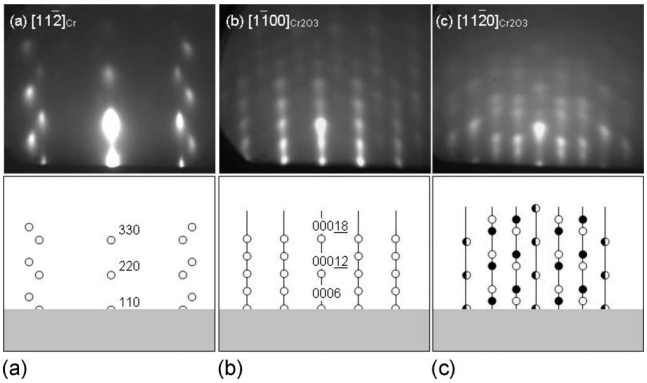

FIG. 1. (a) $[11\bar{2}]$ azimuth RHEED patterns and corresponding key diagram of Cr(110) thin film on Au(111) base layer. (b) $[1\bar{1}00]$ azimuth and (c) $[11\bar{2}0]$ azimuth RHEED patterns and corresponding key diagrams of α-$Cr_2O_3(0001)$ film. Open and closed circles in key diagram represent different sets of diffraction from the twin domains.

In order to determine the crystallographic orientation relationship among the α-$Cr_2O_3(0001)$ film, the Au(111) base layer, the Si(111) substrate, and the in-plane XRD profiles were measured. Figure 2 shows the in-plane XRD profiles of (a) α-$Cr_2O_3(10\bar{1}4)$, (b) Au(200), and (c) Si(400), respectively. In Fig. 2(a), the diffraction peaks with sixfold symmetry are clearly observed. Since $(10\bar{1}4)$ has threefold sym-

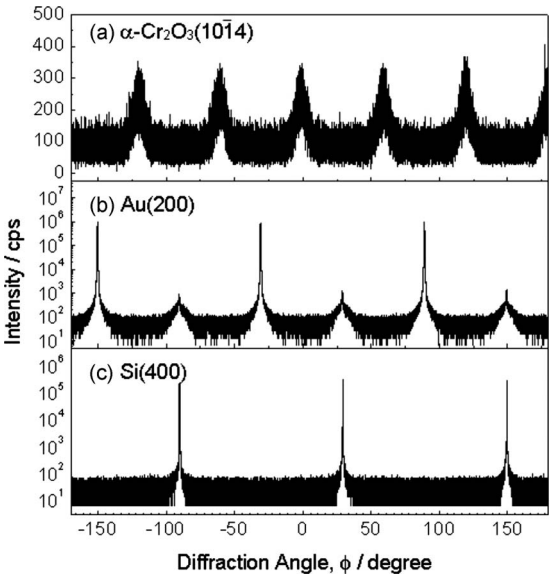

FIG. 2. In-plane XRD profiles of (a) α-Cr_2O_3(0001), (b) Au(111), and (c) Si(111) substrates, respectively. The diffraction conditions were set to the Bragg conditions for (a) α-Cr_2O_3(1$\bar{1}$04), (b) Au(200), and (c) Si(400), respectively.

metry around the (0001) pole for single-crystalline α-Cr_2O_3, the obtained results show the formation of twin domains, in agreement with the RHEED observation. The diffraction peaks from Au(200) show sixfold symmetry, thus Au(111) also has a the twinned structure [Fig. 2(b)]. However, the diffraction intensity is different for the two sets of diffraction peaks, meaning that the twin domains of Au(111) have different volumes. On the contrary, as shown in Fig. 2(a), the intensity of the two sets of diffraction peaks from α-Cr_2O_3(10$\bar{1}$4) is almost the same. Thus, the twinning in α-Cr_2O_3 did not originate from the twin structure of the underlying Au(111), but is an inherent feature of α-Cr_2O_3.

Concerning the diffraction peak position, one set of Au(200) diffraction peaks with weak intensity is located at the same position as the diffraction peaks from Si(400) and the other set deviates by 60° from that of Si(400) [Fig. 2(c)]. Furthermore, the diffraction peaks from α-Cr_2O_3(10$\bar{1}$4) deviate by 30° from Au(200) diffraction peaks. From these relationships, the crystallographic orientation relationships among the α-Cr_2O_3(0001) film, the Au(111) base layer, and the Si(111) substrate are determined as follows.

$$\alpha\text{-}Cr_2O_3(0001)[1\bar{1}00] \parallel Au(111)[1\bar{1}0] \parallel Si(111)[1\bar{1}0],$$

$$\alpha\text{-}Cr_2O_3(0001)[11\bar{2}0] \parallel Au(111)[11\bar{2}] \parallel Si(111)[11\bar{2}].$$

The obtained epitaxial relationship is schematically drawn in Fig. 3. In this orientation relationship, the lattice misfit of 0.8% between α-Cr_2O_3 and Au is obtained for the above two directions, assuming the bulk lattice parameters. Although the crystal structure of our α-Cr_2O_3(0001) film is sufficient to align the spin direction at the interface, the surface of our α-Cr_2O_3(0001) thin film is not very smooth. The surface roughness of about 2.4 nm is obtained by AFM observation with a 500×500 nm^2 scan size (not shown). Thus, the Cr spin direction at the interface would be uncompensated, contrary to the ideal termination of α-Cr_2O_3(0001).

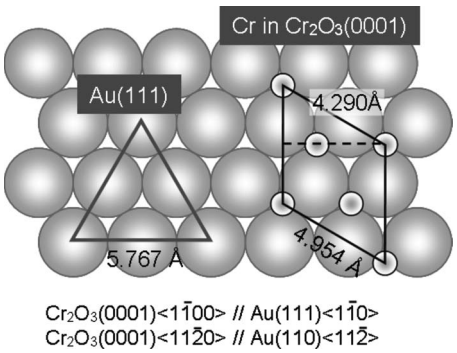

FIG. 3. Schematic of the epitaxial relationship of α-Cr_2O_3(0001) and the Au(111) surface. The corresponding lattice misfit is 0.8%, assuming the bulk lattice parameters.

Figure 4 shows RHEED patterns of ultrathin Co film grown on α-Cr_2O_3(0001) film. For the 2.3-nm-thick and 1.0-nm-thick Co films, the diffraction spots from fcc-Co(111) are clearly observed. Thus, Co grows epitaxially on α-Cr_2O_3(0001) film. In RHEED patterns, the diffraction spots from α-Cr_2O_3(0001) are also observed, even for 2.3-nm-thick Co film, indicating that the α-Cr_2O_3(0001) surface is still exposed within the electron penetration depth. The diffraction spots from α-Cr_2O_3(0001) are clearer in the 1.0-nm-thick Co film than in the 2.3-nm-thick Co film. This is because ultrathin Co film is discontinuous in the ultrathin regime as a result of island growth. The island growth of metal ultrathin film is generally observed on the oxide surface[1,11] owing to the lower surface energy of oxide than that of metal. In addition to the intrinsic feature of island growth, the rough surface of our α-Cr_2O_3(0001) might hinder the formation of a continuous structure.

IV. TEMPERATURE DEPENDENCE OF MAGNETIZATION

α-Cr_2O_3 possesses uniaxial magnetic anisotropy and its Néel axis is the *c*-axis. As mentioned above, our α-Cr_2O_3 film has the ⟨0001⟩ orientation perpendicular to the film sur-

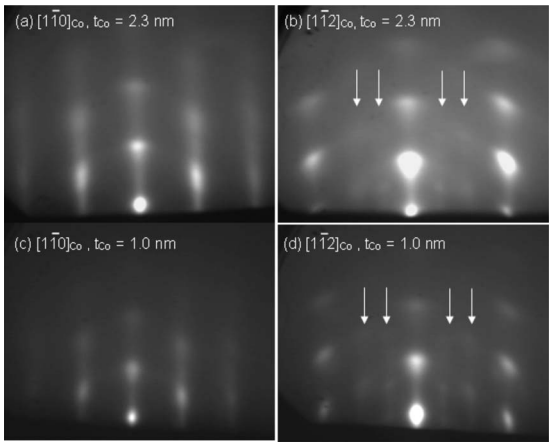

FIG. 4. RHEED patterns of ultrathin Co films. Co thickness is [(a) and (b)] 2.3 nm and [(c) and (d)] 1.0 nm. Electron incidence is [(a) and (c)] [1$\bar{1}$0] and [(b) and (d)] [11$\bar{2}$]. The white arrows in (b) and (d) represent the diffraction position from α-Cr_2O_3(0001).

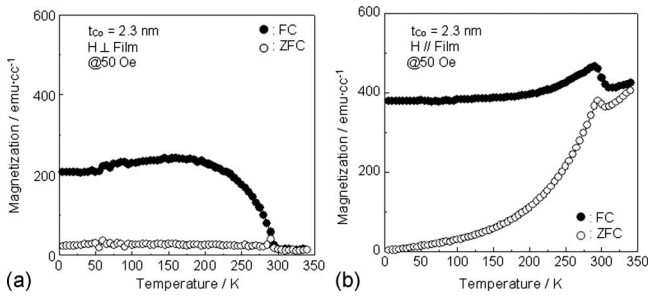

FIG. 5. Temperature dependence of magnetization of 2.3-nm-thick Co film on α-Cr_2O_3(0001). The applied field strength is 50 Oe. The field direction is (a) perpendicular and (b) parallel to the film plane. The closed and open circles represent the results after FC and ZFC, respectively.

face and thus the Cr spins point normal to the interface. Owing to this spin alignment, the magnetic properties of Co on α-Cr_2O_3(0001) film might be affected by the field direction relative to the Cr spin direction. In the following, we show the effect of the Cr spin on the anisotropic magnetic behavior of Co.

Figure 5 shows the temperature dependence of the magnetization of 2.3-nm-thick Co film under a magnetic field of 50 Oe. For the applied field direction perpendicular to the film plane [Fig. 5(a)], the magnetization after FC gradually increases with increasing temperature, starts to decrease at around 200 K, and drops to zero at 295 K, which is the Néel temperature of our α-Cr_2O_3 film. Instead, the magnetization after ZFC is almost zero in the entire temperature range except for the small peak at 295 K. On the other hand, for the applied field direction parallel to the film plane [Fig. 5(b)], the magnetization after both FC and ZFC increases with increasing temperature, except for the peak at 295 K. These features are interpreted by considering the collinear exchange coupling of Co to the Cr spin. As described in Sec. II, the cooling procedures were conducted from 340 K, above the Néel temperature of bulk α-Cr_2O_3. Thus, the Cr spin direction at the interface below the Néel temperature is determined by the competition between magnetocrystalline anisotropy and the magnetization direction of Co via exchange coupling. The magnetocrystalline anisotropy of Cr_2O_3 forces the spins to point perpendicular to the film plane. Hence, when the sample is cooled in a magnetic field perpendicular to the film plane, the direction of magnetocrystalline anisotropy and the magnetization direction of ultrathin Co film are coincident with each other. Consequently, the Cr spin direction at the interface in each Cr_2O_3 grain is aligned, causing the coupling direction of Co to Cr to align. The aligned coupling of Co to Cr forces the Co magnetization to point to the coupled direction, giving rise to the large magnetization perpendicular to the film surface below the Néel temperature. With increasing temperature and weakening antiferromagnetic order of Cr spin, the Co magnetization perpendicular to the film decreases because of the weakened magnetic coupling. At the Néel temperature when the antiferromagnetic order is destroyed, the Co magnetization lies in the film plane owing to the in-plane shape anisotropy. In fact, as shown in Fig. 5(b), the large magnetization remains above the Néel temperature while the magnetization becomes almost zero perpendicular to the film. When the sample is

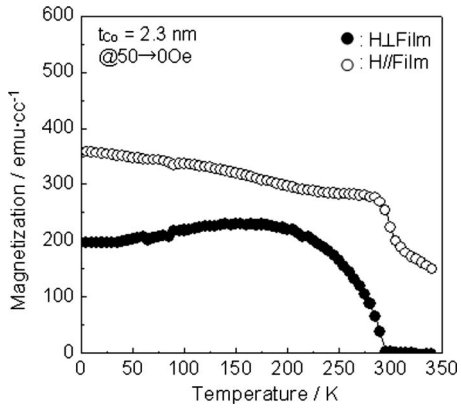

FIG. 6. Temperature dependence of TRM of 2.3-nm-thick Co film on α-Cr_2O_3(0001). The closed and open circles represent the results for the applied field directions perpendicular and parallel to the film plane, respectively.

cooled in zero field, the antiferromagnetic spin direction of Cr_2O_3 grains should randomly be up or down because of the orthogonal alignment of magnetocrystalline anisotropy and Co magnetization. As a result, the coupling direction also becomes random and, hence, the Co magnetization after ZFC is almost zero. When the sample is cooled in the in-plane magnetic field, the Cr spin cannot lie in the field direction because of the magnetocrystalline anisotropy and the collinear coupling of Co and Cr is not achieved.

The temperature dependence of remanent magnetization supports the above discussion because the effect of magnetic anisotropy and exchange coupling become more prominent in the remanent state. Figure 6 shows the temperature dependence of TRM perpendicular and parallel to the film plane. As clearly seen, in the perpendicular direction, TRM is almost the same as the magnetization after FC below the Néel temperature, meaning that the decrease in magnetization upon removing magnetic field is minimal. Above the Néel temperature, TRM become zero due to the absence of the influence of Cr spins. On the contrary, TRM parallel to the film plane monotonically decrease with increasing temperature. These results indicate that the Co magnetization is stabilized in the parallel direction to the Cr spin by the collinear coupling.

The 1.0-nm-thick Co film provides results further supporting the collinear coupling of Co spin and Cr spin. The temperature dependences of magnetization after FC in perpendicular and parallel directions to the film plane are shown in Fig. 7. Similar to the 2.3-nm-thick Co film, the magnetization perpendicular to the film increases gradually with increasing temperature and drops to zero at the Néel temperature. However, the distinct difference upon decreasing Co thickness is that the magnetization perpendicular to the film plane, i.e., parallel to the Cr spin, is larger than that parallel to the film plane. For the case of 2.3-nm-thick Co film, the large in-plane shape anisotropy forces the magnetization to be in plane. Instead, the in-plane shape anisotropy decreases since the 1.0-nm-thick Co film possesses a more distinct discontinuous structure than the 2.3-nm-thick Co film. As a result, the decreased shape anisotropy and the collinear coupling of Co spin to Cr spin give rise to the larger magnetization in the perpendicular direction.

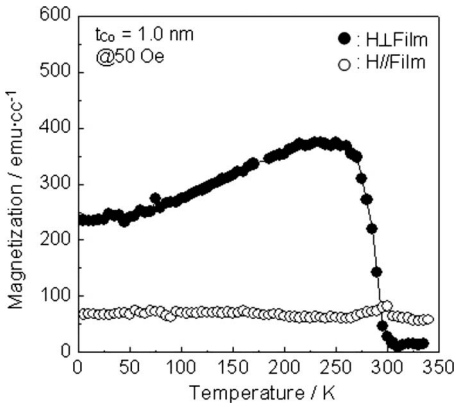

FIG. 7. Temperature dependence of magnetization of 1.0-nm-thick Co film on α-Cr_2O_3(0001). The applied field strength was 50 Oe. Closed and open circles represent the results for the applied field directions perpendicular and parallel to the film plane, respectively.

V. EXCHANGE BIAS AND COERCIVITY

It is expected that the collinear coupling of Co and Cr at the interface causes the exchange bias in the coupled direction. The magnetization curves of 2.3-nm-thick Co film are shown in Fig. 8. The measurement temperature is 5 K. As clearly seen, the exchange bias of about 410 Oe is observed in the perpendicular direction to the film [Fig. 8(a)], while no exchange bias is observed in the direction parallel to the film [Fig. 8(b)]. These results mean that the exchange bias acts in the direction parallel to the Cr spin. Contrary to our results, an exchange bias parallel to the film plane for polycrystalline NiFe on α-Cr_2O_3(0001) has been previously reported.[4] The difference between our results and the previous report might be the exchange coupling direction of the ferromagnetic layer and α-Cr_2O_3(0001). As described in Fig. 4, our ultrathin Co film has the (111) orientation perpendicular to the film. Since the ⟨111⟩ direction of fcc Co is the magnetic easy axis, we believe that the collinear coupling of Co and Cr is promoted by the coincident directions of the magnetic easy axis of ferromagnetic film and the Néel axis of antiferromagnetic film.

In Fig. 8, it is also seen that the smaller coercivity and the larger saturation field are observed in the direction perpendicular to the film than those parallel to the film, although the exchange bias is only observed in the former direction. This is probably due to the in-plane shape anisotropy described in the previous section. Nevertheless, even for 1.0-nm-thick Co film in which the in-plane shape anisotropy should be reduced, the above characteristics are still observed (not shown). These results imply that, in addition to the in-plane shape anisotropy, another type of exchange coupling, for example, the biquadratic coupling (spin-flop coupling), might act at the interface,[13] which contribute to the coercivity enhancement. In other words, our results indicate that two types of magnetic coupling are in effect at the interface and these couplings contribute to either exchange bias or coercivity enhancement in a different manner, i.e., collinear coupling contributes to exchange coupling and biquadratic coupling contributes to coercivity enhancement. Different origins of the exchange bias and the coercivity enhancement are also suggested in the past report of the study using polycrystalline NiFe/$Cr_2O_3(1\bar{1}02)$.[4]

Concerning the biquadratic coupling at the interface, Hu *et al.*[14] theoretically reported that the exchange bias field decreases nonmonotonically with increasing temperature when both collinear and biquadratic couplings are in effect at the interface, while it shows the monotonic decrease when only collinear coupling is in effect. Thus, the change of exchange bias with temperature will provide further information on interface coupling. Figure 9(a) shows the changes in exchange bias with temperature. The exchange bias field is almost constant below 50 K (150 K) for 2.3-nm-thick (1.0-nm-thick) Co films and it vanishes at the blocking temperature. It is clear that the exchange bias in our system shows a nonmonotonic decrease with temperature, in agreement with the theoretical prediction for biquadratic coupling. In addition, as shown in Fig. 9(b), the coercivity starts to increase around the blocking temperature and shows a peak below the Néel temperature. While this feature is explained by the thermal activation of magnetic reversal in the antiferromagnetic grains,[15] the theoretical prediction[14] also suggests that the peak of coercivity is generated even when biquadratic coupling acts at the interface.

Although the origin of biquadratic coupling is not always clear, the surface/interface roughness could induce biquadratic coupling through the frustration of antiferromagnetic spins by competing antiferromagnetic exchange interaction between the antiferromagnetic sublattice and fer-

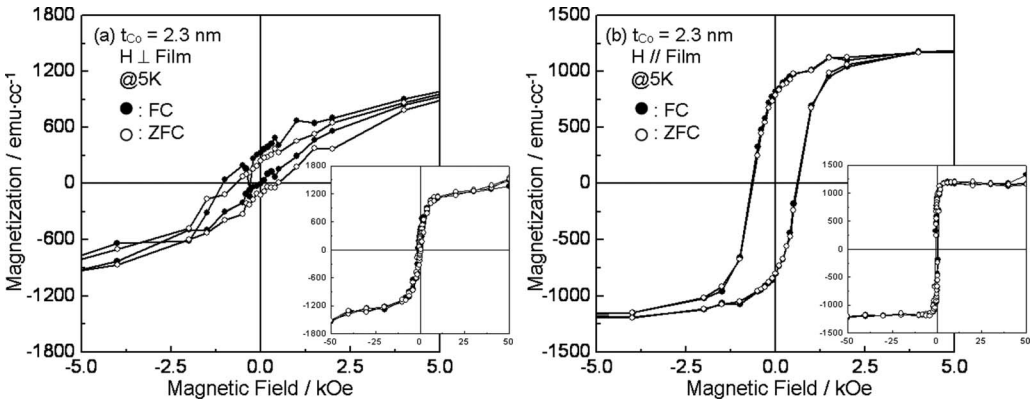

FIG. 8. Magnetization curves of 2.3 nm-thick Co film on α-Cr_2O_3(0001). The applied field direction is (a) perpendicular and (b) parallel to the film plane. Closed and open circles represent the results after FC and ZFC, respectively. Insets show the entire magnetization curve in the range from −50 to 50 kOe.

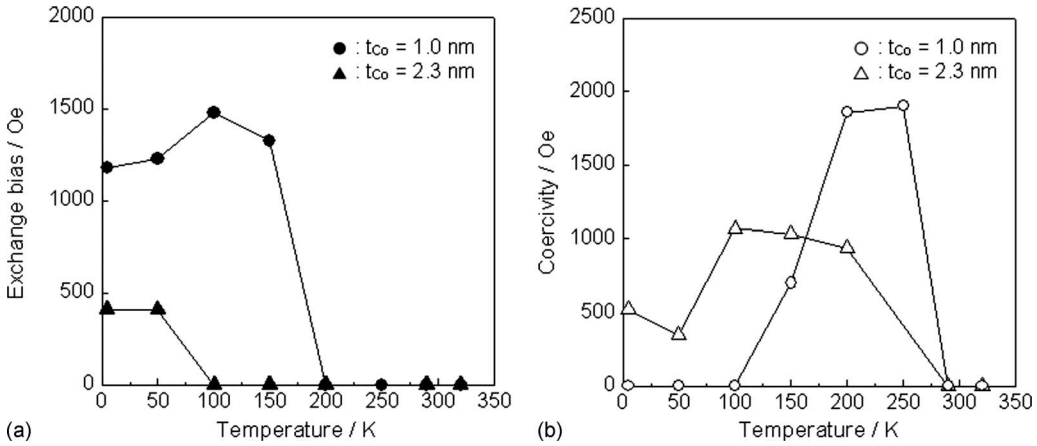

FIG. 9. Temperature dependence of (a) exchange bias field and (b) coercivity of ultrathin Co film on α-Cr_2O_3(0001). The applied field direction is perpendicular to the film plane, namely, parallel to the Cr spin direction. Triangles and circles represent the values for 2.3-nm-thick and 1.0-nm-thick Co films, respectively.

romagnetic spins.[13,16] Actually, our Cr_2O_3(0001) films have the surface roughness of about 2.4 nm, which is not very smooth, as mentioned in Sec. III. We believe that the surface roughness generates the biquadratic coupling in our case. In addition to surface roughness, a different mechanism is proposed for the origin of biquadratic coupling, e.g., higher order contributions from the compensated and uncompensated interfaces,[17] and the superexchange interaction.[8] In order to clarify the details of the origin of biquadratic coupling, it is necessary to improve the interface roughness, at least; further investigation is needed.

Finally, we discuss the change in blocking temperature with Co thickness. In general, the blocking temperature decreases with decreasing thickness since the thinner film is composed of smaller grains. Contrary to this expectation, as shown above (Fig. 9), the blocking temperature of 1.0-nm-thick Co film is higher than that of 2.3-nm-thick Co film. Here, we interpret the results qualitatively on the basis of the thermal fluctuation model.

The change in blocking temperature with the grain size is often discussed using the thermal fluctuation model of antiferromagnets.[15,18,19] In the most proposed model, it is assumed that the grain size of the ferromagnet is larger than that of the antiferromagnet because the ferromagnetic film is assumed to be a continuous film structure. However, in our case, the antiferromagnetic Cr_2O_3(0001) film grows in an epitaxial manner and it has more than ten times larger thickness than the ultrathin Co film. Furthermore, our ultrathin Co film is discontinuous even at the thickness of 2.3 nm. Thus, the grain size of antiferromagnetic Cr_2O_3(0001) film is probably larger than that of ultrathin Co film. Therefore, it is unsuitable to apply existing models to our case, but the essential mechanism would still be applicable. According to the thermal fluctuation model, the blocking temperature is determined by the thermally activated magnetization reversal of antiferromagnetic grains. The magnetization reversal of the antiferromagnet is driven by the combination of thermal activation and torque from the ferromagnet to the antiferromagnet, which is in effect when the magnetization of the ferromagnet reverses. According to Nishioka *et al.*,[19] the torque generated at the interface is expressed as

$$JM_SM_{SA}AC\cos(\theta_i - \mathbf{\Phi}_j), \tag{1}$$

where J is the exchange coupling constant, M_S and M_{SA} are the saturation magnetizations of the ferromagnet and antiferromagnet, respectively, A is the interface area, C is a constant fraction that is related to interface morphology, θ_i is the angle between the magnetic field and interface magnetic moment of the ith antiferromagnetic grain, and Φ_i is the angle between the magnetic field and interface magnetic moment of the jth ferromagnetic grain.

In most models, it is assumed that the ferromagnet is the continuous film and that the magnetization of the ferromagnet is uniform. Then, Φ_i in Eq. (1) is replaced by Φ. In this case, the torque that drives the magnetization reversal of antiferromagnetic grains is clearly governed by A [Fig. 10(a)].

On the other hand, when the ferromagnetic layer is discontinuous, the magnetization direction of the ferromagnet is nonuniform, causing a variation in Φ_i. Furthermore, when the antiferromagnetic grains are sufficiently larger than the ferromagnetic grains, as in our samples, the magnetization direction of the antiferromagnet, θ_i, can be replaced by θ. In this case, the torque on the antiferromagnetic grain is also nonuniform and the torque from each ferromagnetic grain is compensated on individual antiferromagnetic grains [Fig. 10(b)]. The compensation decreases the effective torque on individual antiferromagnetic grains and thus the driving force of the magnetization reversal of the antiferromagnet also decreases, causing a higher blocking temperature. In accordance with this mechanism, the compensation of torque at the interface is promoted by decreasing the ferromagnetic grain size. Hence, the observed increase in the blocking temperature with decreasing Co thickness can be explained as in the above discussion.

VI. SUMMARY

We investigated the magnetic coupling at the interface between ultrathin Co film and antiferromagnetic Cr_2O_3(0001) film, as well as the structures of Cr_2O_3 film and ultrathin Co film. We successfully fabricated α-Cr_2O_3(0001) film on a Au(111) base layer, which is the system to be

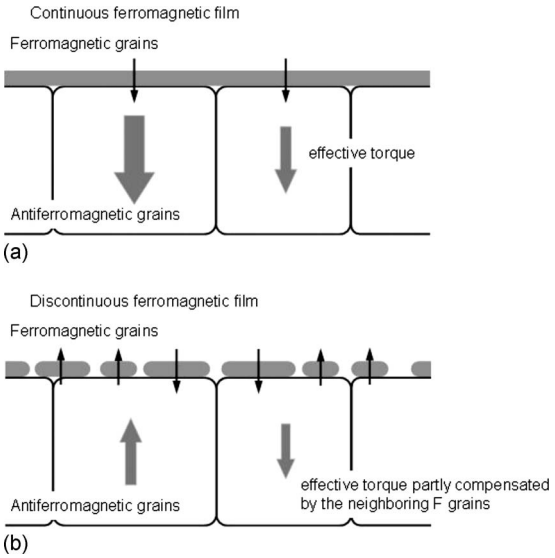

FIG. 10. Drawing of the effective torque driving the magnetization reversal of antiferromagnetic grains for the ferromagnetic film with (a) continuous and (b) discontinuous structures. The thin arrows represent the magnetization direction of Co grains (film) and the torque from the individual Co grains (film). The thick arrows represent the effective torque acting on individual antiferromagnetic grains. For the continuous ferromagnetic film, the magnetization is uniform, thus the torque on individual antiferromagnetic grains depends on the grain size of antiferromagnet. On the other hand, for the discontinuous ferromagnetic film, the torque becomes nonuniform owing to the reversal field distribution of ferromagnetic grains, thus the torque on individual antiferromagnetic grains decreases effectively (see text).

utilized in magnetoelectronic applications. Although the surface of the fabricated α-$Cr_2O_3(0001)$ film is not very smooth, the crystalline quality is sufficient to exhibit antiferromagnetic features. The antiferromagnetic nature of α-$Cr_2O_3(0001)$ film strongly affects the magnetic properties of ultrathin Co film. In the temperature dependence of magnetization, the magnetization of Co is stable in the direction parallel to Cr spin below the Néel temperature. The stable magnetization parallel to Cr spin indicates the collinear coupling of Co and Cr spins. The collinear coupling results in an exchange bias in the direction parallel to Cr spin, while the exchange bias is not observed in the direction perpendicular to Cr spin. In addition, larger coercivity and the lower saturation field are obtained in the perpendicular direction to Cr spin, even for 1.0-nm-thick Co film in which the discontinuous structure of Co film is conspicuous. These results indicate that biquadratic coupling acts at the interface. The temperature dependences of exchange bias field and coercivity also indicate the coexistence of collinear and biquadratic coupling at the interface.

ACKNOWLEDGMENTS

We thank Dr. Fumiyoshi Kirino of Tokyo National University of Fine Arts and Music for the assistance in the EDX measurement. This study was partly supported by Encouragement of Young Scientists (B) and Priority Assistance for the Formation of Worldwide Renowned Centers of Research—The Global COE Program (Project: Center of Excellence for Advanced Structural and Functional Materials Design) from the Ministry of Education, Culture, Sports, Science and Technology (MEXT), Japan.

[1] Y. Shiratsuchi, M. Yamamoto, and S. D. Bader, Prog. Surf. Sci. **82**, 121 (2007).
[2] Y. Shiratsuchi, Y. Endo, M. Yamamoto, and S. D. Bader, J. Appl. Phys. **97**, 10J106 (2005).
[3] V. Skumryev, S. Stoyanov, Y. Zhang, G. Hadjipanayis, D. Givord, and J. Noués, Nature (London) **423**, 850 (2003).
[4] J. Dho, M. G. Blamire, and E. O. Chi, Phys. Rev. B **72**, 224421 (2005).
[5] L. M. Corliss, J. M. Hantings, R. Nathans, and G. Shirane, J. Appl. Phys. **36**, 1099 (1965).
[6] P. Borisov, A. Hochstrat, X. Chen, W. Kleemann, and C. Binek, Phys. Rev. Lett. **94**, 117203 (2005).
[7] J. Nogués and I. K. Schuller, J. Magn. Magn. Mater. **192**, 203 (1999).
[8] A. E. Berkowitz and K. Takano, J. Magn. Magn. Mater. **200**, 552 (1999).
[9] J. Dormann, D. Fiorani, and E. Tronc, Adv. Chem. Phys. **98**, 283 (1997).
[10] T. R. MuGuire, E. J. Scott, and F. H. Grannis, Phys. Rev. **102**, 1000 (1956).
[11] Y. Shiratsuchi, T. Nakatani, S. Kawahara, and R. Nakatani, J. Phys.: Conf. Ser. **165**, 012034 (2009).
[12] H. Brficle, J. Vancea, R. Lecheler, G. Reiss, and H. Hoffmann, Thin Solid Films **250**, 56 (2003).
[13] N. C. Koon, Phys. Rev. Lett. **78**, 4865 (1997).
[14] J.-G. Hu, G. Jin, A. Hu, and Y.-Q. Ma, Eur. Phys. J. B **40**, 265 (2004).
[15] M. D. Stiles and R. D. McMicheal, Phys. Rev. B **63**, 064405 (2001).
[16] J. C. Slonzewski, Phys. Rev. Lett. **67**, 22 (1991).
[17] R. L. Stamps, J. Phys. D **33**, R247 (2000).
[18] E. Fulcomer and S. H. Charap, J. Appl. Phys. **43**, 4190 (1972).
[19] K. Nishioka, C. Hou, H. Fujiwara, and R. D. Metzger, J. Appl. Phys. **80**, 4528 (1996).